



REEL Demo – Romande Energie ELectric network in local balance Demonstrator

Deliverable: 3d3 Design and test of distributed DSM
algorithms that use communication and new forecasting
models

Demo site: Chapelle

Developed by

Lorenzo Nespoli, ISAAC, SUPSI

Vasco Medici, ISAAC, SUPSI

Roman Rudel, ISAAC, SUPSI

[Canobbio, 30.09.2020]

1 Description of deliverable and goal

This deliverable was originally linked to the experimental demonstration of decentralized demand-side management (DSM) control strategies and the assessment of their performances in the context of the Romande Energie Demo site. Due to technical issues, it was not possible to set up a distributed demand side control demonstrator managing the demand side of a high number of residential clients. For this reason, the focus of the proposal switched to the performance comparison of different DSM strategies based on simulation results, with a deeper focus on different forecasting techniques than previously anticipated.

1.1 Executive summary

In this deliverable, the effectiveness of different forecasting models was tested, and assessed in combination with a model predictive control, in closed loop. The evaluation was done both in terms of forecasting accuracy and in terms of economic results of different combinations of forecasters and control algorithms. We restricted the study to the control of distributed electric batteries for demand-side management applications. We tested 5 different forecasters, namely a Holt-Winters based model and different flavors of Gradient Boosted Trees. Two coordination schemes were tested, associated with two alternatives tariff schemes: an implicit coordination, and an explicit coordination scheme. In both the approaches, the final costs for the end-users are only determined by the aggregated energy consumption and production of a group of users, that is, the final price is generated by an automated market maker mechanism. In the implicit approach coordination is achieved without communication, but only using the forecasts of the energy prices as guidance (which depend on future energy consumption and production). The explicit coordination additionally uses an iterative coordination scheme obtained formulating the welfare maximization problem as a non-cooperative game, through distributed optimization; in this case, the final prices for the end-users are generated through the re-partition of a system-level economic objective among the users; this re-partition depends on how much each user helped in the minimization of this system-level objective.

The performances were evaluated on a simulation environment replicating the LIC pilot¹, a self-consumption community located in Lugaggia, a small village near Lugano. The simulation environment simulates thermo-electric appliances, building heating systems and thermal dynamics, and power flow on the local low voltage grid.

Results show how the first step ahead accuracy has a higher impact on the economic results under both the implicit and explicit coordination and remuneration schemes. Switching from the implicit coordination to the explicit one shows a slight increase in the financial performances; this performance difference is expected to increase with increasing penetration of controlled batteries since the implicit coordination cannot

¹<https://lic.energy/>

fully handle correlations in user's control actions.

Additionally, we relaxed the constraint for which the batteries can only charge or discharge from and into the households' electric main. This increases the feasible space of the controller, leading to better economic results. As a consequence, the accuracy of the forecasters on steps ahead beyond the first one increases its importance on the final economic results.

1.2 Research question

- How accurately can we forecast residential power profiles? Residential power profiles are characterized by high variance and low signal to noise ratios. Residential buildings with significant electric loads like electric boilers and heat pumps don't show a perfect seasonality, and severely unbalanced distribution gets hard to predict.
- Does an increased accuracy on the whole forecast horizon reflects in an increase of control performances? Despite this being a common assumption in control problems exploiting systems with an energy buffer, the accuracy of the forecasts at different timesteps is not usually investigated in terms of performances.
- How worse is an implicit coordination mechanism compared to an iterative coordination scheme?

1.3 Novelty of the proposed solutions compared to the state-of-art

Accuracy of forecasters is not usually compared in closed-loop control, but rather in open-loop through KPIs on the prediction accuracy. In this deliverable, we performed a closed-loop comparison through different coordination and remuneration schemes. Forecasters were selected among different parametric and non-parametric models which already proved to deliver good results in the energy demand and production prediction tasks.

1.4 Description

1.4.1 Coordination cases

Beside comparing different forecast algorithms, two different approaches were compared for the control of distributed electrochemical storage:

1. Explicit control: it is based on the decentralized energy market presented in [1] and [2]. The approach explicitly models a welfare maximization problem with coupling constraints representing power and voltage constraints in a local distribution grid.
2. Implicit control: this approach is based on dynamic prices which are formed through simple price formation rules, which try to minimize the impact of

the distributed energy resources in the grid and try to increase overall self-consumption. The agents are indirectly coordinated by forecasting the dynamic price and optimizing for their costs.

Explicit control The problem can be mathematically formulated as a variant of the so called sharing problem [3]:

$$\begin{aligned} \underset{u \in \mathcal{U}}{\operatorname{argmin}} \quad & e(S_{\emptyset} u) + \sum_{i=1}^N c(u_i) \\ \text{s.t.} \quad & A_{\lambda} u \leq b \end{aligned} \quad (1)$$

where u_i are the actions associated with the agent i , $\mathcal{U} = \prod_{i=1}^N \mathcal{U}_i$ is the Cartesian product of the flexible users feasible sets, $e(u)$ is a system level objective which defines the business model, $c(u_i)$ are the costs of each flexible user in the business as usual case, and $u = [u_1^T, \dots, u_N^T] = [u_i]_{i=1}^N$ is the vector of the concatenated actions of all the flexible users. Here A_{λ} is a constraint matrix, taking into account the linear influence of the end users' powers on the problem constraints, and b encodes box constraints limits on the power and voltages at specified grid's nodes.

A notable business model is the one of energy communities, or self consumption community (SCC), for which the billing is done at the point of common coupling (PCC) with the main grid. In this case the function $e(u)$ is the surplus that the agent community has in paying the energy at the point of common coupling with the electrical grid:

$$e(x) = c \left(\sum_{i=1}^N u_i \right) - \sum_{i=1}^N c(u_i) \quad (2)$$

where $u_i \in \mathbb{R}^T$ is the vector of total power of the i th agent, $c(\cdot)$ is the energy cost function defined as:

$$c(p_t) = \begin{cases} p_{b,t} p_t, & \text{if } p_t \geq 0 \\ p_{s,t} p_t, & \text{otherwise} \end{cases} \quad (3)$$

where $p_{b,t}$ and $p_{s,t}$ are the buying and selling tariffs, respectively, at time t and p is the power at the households' electric main. Decomposing (1) using different repartition weights for the surplus, induces a game with unique generalized variational equilibrium, which can be reached jointly minimizing the utility function of the agents, given by:

$$c_{tot}(u_i, x_{-i}) = c_i(u_i) + \alpha_i e(u) + \lambda_i^T u_i \quad (4)$$

where α is a repartition coefficient for prosumer i , $\lambda_i \in \mathbb{R}^{2T}$ is a vector of Lagrangian multipliers associated with the i th agent.

The α_i coefficient in (4) is intended to promote a truthful report of the users' power forecasts and redistribute the SCC's economic surplus (2), so that the users are

interested in maximizing $e(x)$. In [2] we proposed the following formula for α_i :

$$\alpha_{i,t} = a_{i,t} \frac{\sum_{k=t-\tau}^t |x_{i,k}|}{\sum_{k=t-\tau}^t \sum_{i=1}^N |x_{i,k}|} \quad (5)$$

where τ is a characteristic period (e.g. one week). This is basically a normalized moving average of the consumption (or production) of the i_{th} agent. In other words, the discount experienced by the SCC member is proportional to the produced or consumed kWh. For the numerical experiments carried out in the following sections, we have adopted a different definition which promote fairness: the α_i coefficients are computed using moving averages of the change in the surplus due to the action of the i_{th} agent. In other words, called $e(x_{-i})$ the surplus computed without the action of the i_{th} agent, the α_i are defined as:

$$\alpha_{i,t} = a_{i,t} \frac{\sum_{k=t-\tau}^t \tilde{\alpha}_{i,k}}{\sum_{k=t-\tau}^t \sum_{i=1}^N \tilde{\alpha}_{i,k}} \quad (6)$$

$$\tilde{\alpha}_i = e(x_i) - e(x_{-i}) \quad (7)$$

Implicit control A default rule that allows calculating the price of electricity sold at any time is defined. Users can then react according to this price signal. We will call this mechanism "implicit coordination". Various pricing schemes can be adopted, in this case we opted for a simple and easy to explain one. We define the price formation mechanism using extremely simple and interpretable rules:

- The energy consumed from the external grid shall be paid for as if the consumer were not part of the community.
- The energy consumed from inside the community is paid for at a total price lower than the standard tariff of the energy supplier and DSO, with a discount proportional to the ratio of the total produced and consumed energy.
- The energy injected into the external grid shall be remunerated as if the consumer were not part of the community.
- The energy injected, which is consumed inside the community is remunerated at a price higher than the standard tariff of the energy supplier, with a discount proportional to the ratio of the total consumed and produced energy.

This simple set of rules push flexible users to increase the overall self-consumption. The energy price is calculated using an automated market making (AMM) mechanism, which follows these principles:

- The self-consumed energy is equally split among the community members proportionally to their consumption and production.
- The instantaneous buying and selling prices are dynamic, but for a given time slot they are the same for everyone.

We define the price functions of our AMM mechanism starting from the previously introduced rules, which can be expressed formally as:

$$\begin{aligned} p_b &= (E_c p_b^{BAU} - \min(E_c, E_p)(p_b^{BAU} - p_b^{P2P})) / E_c \\ p_s &= (E_p p_s^{BAU} - \min(E_c, E_p)(p_s^{P2P} - p_s^{BAU})) / E_p \end{aligned} \quad (8)$$

where p_b and p_s are the buying and selling prices generated by the AMM, E_c and E_p are the sum of the energy consumed and produced inside the energy community, while p_b^{BAU} , p_s^{BAU} , p_b^{P2P} and p_s^{P2P} are the buying and selling prices in the Business as Usual (BAU) case and inside the energy community. In such pricing configuration, peers clearly profit from the difference in price between BAU and P2P, but the community administrator also earns money, when energy is self-consumed inside the community. It is important to notice that P2P tariff is applied only to the energy produced by the members of the community, as a consequence it is also in the administrator interest to maximize self-consumption (no conflicting interests between peers and community admin).

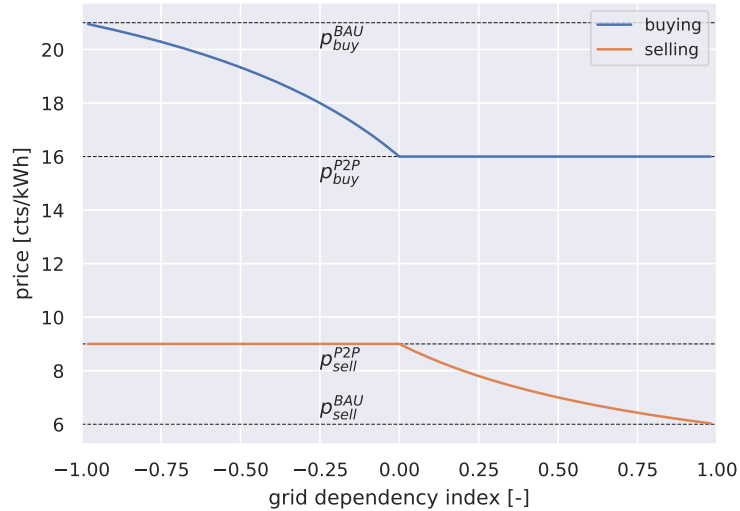


Figure 1: Buying and selling prices as a function of the GDI.

We can develop some intuition on how these prices reduce the variance of the aggregated power profile and maximize self-consumption plotting them as a function of the grid dependence index, defined as:

$$GDI = (E_p - E_c) / (E_p + E_c) \quad (9)$$

The GDI defines how much the community is dependent on the main grid, which provides an infinite reservoir of negative or positive energy. When the GDI is equal to 1, no one is consuming inside the community, while a GDI of -1 indicates that no one is producing. As shown in Fig. 1, the selling price for a net energy producer increases as the GDI moves from 1 to 0, then reaching a plateau. The same is seen

for the buying price for a net consumer, decreasing while the GDI shifts from -1 to 0 , and getting constant thereafter. This means that the community maximizes his welfare when the GDI is 0 , that is when the buying price is minimized and the selling price is maximized for the agents. This means that the community maximizes its welfare when the self-consumption is maximized.

1.4.2 Battery models

The battery controller is supposed to be interfaced with the battery energy management system, returning an estimation of the battery's state of charge and injected and withdrawn power, into and from the battery. In this setting, the battery can be considered as a one state fully observed system and applying the MPC is straightforward. The formulation of the battery control algorithm for the implicit coordination is based on the work published in [2], and has been further improved to decrease the overall computational time, exploiting a new formulation for enforcing mutual exclusivity in charging and discharging operations. We report it in the following. Called $u = [p_{ch}^T, p_{ds}^T]^T \in \mathbb{R}^{2T}$ the vector of concatenated decision variables for the control horizon T , where p_{ch} and p_{ds} are the battery charging and discharging power, respectively, $\tilde{u} = [p_{ch}, p_{ds}] \in \mathbb{R}^{T \times 2}$ being the same vector reshaped in a 2 columns matrix, $\hat{p} \in \mathbb{R}^T$ being the forecasted power at household's main for the next control horizon, $y \in \mathbb{R}^T$, $s_{ch} \in \mathbb{R}^T$, $s_{ds} \in \mathbb{R}^T$ being three auxiliary variables, we seek to solve the following problem:

$$u^*, y^* = \underset{u, y}{\operatorname{argmin}} \sum_t^T y_t + \|s_{ch}\|^2 + \|s_{ds}\|^2 \quad (10)$$

$$x_{t+1} = Ax_t + B\tilde{u}^T \quad (11)$$

$$y \succcurlyeq p_b (\tilde{u}[1, -1]^T + \hat{p}) \quad (12)$$

$$y \succcurlyeq p_s (\tilde{u}[1, -1]^T + \hat{p}) \quad (13)$$

$$x \in [x_{\min}, x_{\max}] \quad u \in [u_{\min}, u_{\max}] \quad (14)$$

$$s_{ch}, s_{ds} \succcurlyeq 0 \quad (15)$$

$$s_{ch} \succcurlyeq -\hat{p} \quad s_{ds} \succcurlyeq \hat{p} \quad (16)$$

$$u \preccurlyeq [s_{ch}, s_{ds}] \quad (17)$$

where \succcurlyeq stands for \succcurlyeq_{R_+} , indicating element-wise inequalities, $p_b \in \mathbb{R}^T$ and $p_s \in \mathbb{R}^T$ are the business as usual buying and selling prices. We start analyzing the objective function (10) term-wise. The first summation in (10) represents the total cost of the agent in the business as usual case. For prosumers, the cost function can be either positive or negative, depending on the overall power at their household's main and can be expressed as in equation (3). The cost can be thought of as the maximum over two affine functions (the first and second line of equation (3), respectively). Equations (12),(13) constraint y to live in the epigraph of the maximum of these two affine functions. Minimizing y then guarantees that its value at the optimum, y^* , will

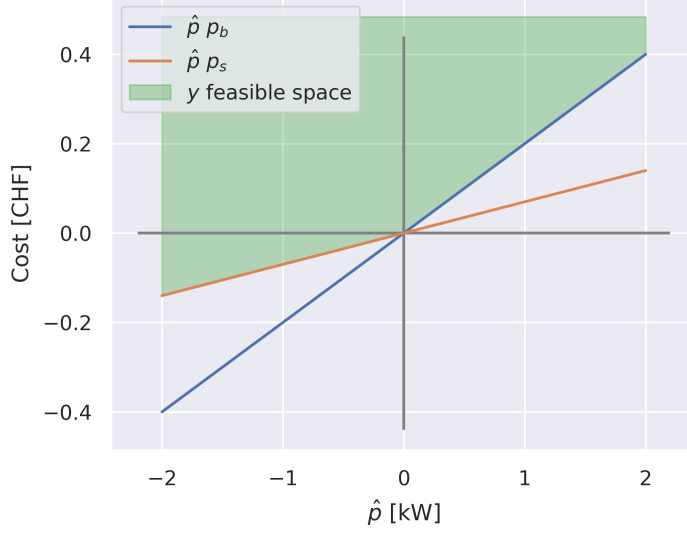


Figure 2: Visual explanation of the scope of the y variable. When linearly penalized, y is pushed to its feasible space's lower borders, collapsing on the cost function $c(p)$ in (3)

lie on the epigraph's lower boundary (and will thus represent the prosumer's total costs), as shown in figure 2. Equation (11) describes the battery's dynamics. $A \in \mathbb{R}_+$ and $B \in \mathbb{R}_+^{1 \times 2}$ are the discrete dynamics matrices obtained by the continuous one through exact discretization [4]:

$$\begin{aligned} A &= e^{A_c dt} \\ B &= A_c^{-1} (A_d - I) B_c \end{aligned} \quad (18)$$

where $A_c = \frac{1}{\eta_{sd}}$ and $B_c = [\eta_{ch}, \frac{1}{\eta_{ds}}]$, and η_{sd} , η_{ch} and η_{ds} are the characteristic self-discharge constant, charge and discharge efficiencies, respectively. Since B_c defines an asymmetric behaviour in charging and discharging (even with equal charging/discharging coefficients), solving the battery scheduling requires to use two different variables for the charging and discharging powers, p_{ch} and p_{ds} . When considering grid constraints, the battery can try to dissipate energy through round-trip efficiency to help respect negative grid constraints (when there is an excessive PV generation), so that in this case we need explicit binary complementary constraints for enforcing mutual exclusivity (the battery cannot charge and discharge at the same time). This can be obtained in three ways: explicitly modeling the bi-linear constraint $p_{ch}p_{dc} = 0$, introducing a binary variable and model it through big M formulation, or trying to restrict their feasible space. The first way will make the problem non-linear, while the second will turn it into a MIQP introducing a binary variable; as both options will increase the computational time, we introduced a new formulation exploiting the third way. Charging and discharging powers are effec-

tively separated using the auxiliary variables s_{ch} and s_{ds} . The feasible space of s_{ds} is constrained to be the epigraph of the maximum between 0 and the forecasted power at the main. As shown in figure 3 for the case of s_{ds} , the equations (15) and (16) constrain these auxiliary variables to live in the positive half-plane and to be higher than the power profile at main (or its negative value for s_{ch}). When s_{ch} is quadratically punished, it will shrink on the lower boundary of the epigraph, (orange line in the second panel of figure 3). Its optimal value can then be used to define the feasible regions of the battery charging power, as done by equation (17). The same reasoning done in figure 3 for the discharging power can be applied to define the feasible regions for the battery's charging power; this will result in two disjoint feasible sets for the charging and discharging powers.

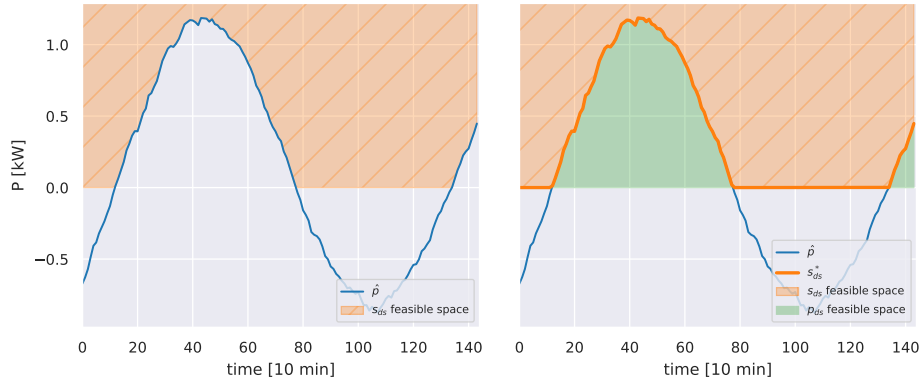


Figure 3: Visual explanation of the change in the feasible space for the discharging power.

The presented problem formulations for the battery, (10), minimizes the end users' business as usual costs. These can be adapted to solve the decomposed sharing problem (1) simply modifying the part of the objective function representing the end users' costs and altering the feasible space for the charging and discharging powers. The total costs for the In particular, using the expression presented in section 1.4.1 for the total costs for the agent, the economic cost of the agent becomes:

$$c_{tot,i} = c(u_i) + \alpha_i e(u) \quad (19)$$

$$= \alpha_i c \left(\sum_{i=1}^N u_i \right) + (1 - \alpha_i) c(u_i) \quad (20)$$

This cost function must be augmented with the Lagrangian multipliers coming from the decomposition of problem (1):

$$c_{tot,i} = \alpha_i c \left(\sum_{i=1}^N u_i \right) + (1 - \alpha_i) c(u_i) + \lambda_i^T u \quad (21)$$

$\lambda_i = [\lambda_{i,ch}^T, \lambda_{i,ds}^T]^T \in \mathbb{R}^{2T}$ being the vector of Lagrangian multipliers associated to the

i_{th} agent. Briefly speaking λ_i is a filtration of the overall λ induced by A_λ in (1). More details about this filtration process can be found in [2, 1]. In order to allow batteries to charge and discharge when system-level constraints are violated, we must further modify the feasible space of p_{ch} and p_{ds} in (10). In particular, equations (16) and (17) become:

$$s_{ch} \succcurlyeq -\hat{p} + M\lambda_{i,ch} \quad (22)$$

$$s_{ds} \succcurlyeq -\hat{p} + M\lambda_{i,ds} \quad (23)$$

$$(24)$$

Here M is a big constant, that we set to $1e6$ in the simulations. An example of change in the feasible space of p_{ds} is shown in figure 4.

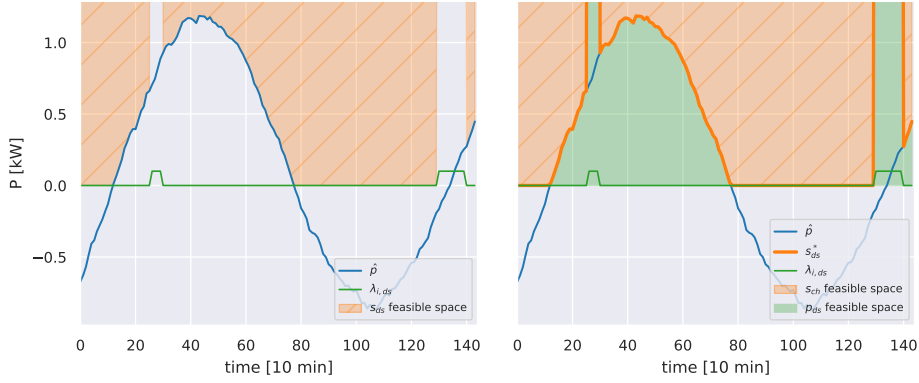


Figure 4: Visual explanation of the change in the feasible space for the discharging power, when s_{ds} is modified taking into account the Lagrangian associated to the battery's charging power $\lambda_{i,ds}$.

Finally, using the preconditioned forward backward formulation, agents perform a gradient descent step in the direction of the negative gradient of the system level cost. This can be formulated as the minimization of the linearization of the system level cost around the previous state, plus a quadratic punishment on the action at the previous iteration; more details on this equivalence can be found in [2]. Replacing the agent cost with the auxiliary variable y as in (10), the final objective function (for the battery) then becomes:

$$\alpha_i \nabla c \left(\sum_{i=1}^N u_{i,pre} \right)^T u_i + (1 - \alpha_i) \sum_{i=1}^T y + \lambda_i^T u + \rho_d \|u - u_{pre}\|^2 + \|s_{ch}\|^2 + \|s_{ds}\|^2 \quad (25)$$

where $u_{i,pre}$ are the agents actions at the previous iteration.

1.4.3 Forecasting models for DSM

Residential power profiles are characterized by high variance and right-skewed data. This is due to the non-synchronous activation of loads and the presence of devices with a predominant power consumption (e.g. heat pumps and electric boilers) w.r.t. the other appliances. The activation of these loads doesn't usually have a strict seasonality effect; for example, heat pumps are usually characterized by several turn on events during the day, but the activation time seldom coincide with the one of the previous day. This makes the power profile hard to forecast.

In the following we describe the forecasting models that we have used for the closed loop comparison. We focused on methods which have already proved to be accurate in forecasting 24 hours ahead residential power profiles. In particular we tried to improve the performance of the methods that were tested in [5] and [6], and focused on the Holt-Winters method and on different forecasting techniques exploiting gradient boosted models (GBM), a family of competition-winning, general-purpose, non-parametric regressors, which exploit sequential model fitting and gradient descent to minimize a specific loss function. For these latter models, we applied a preliminary causal embedding of the explanatory variables, in order to capture seasonal effects. Starting from the original time series $s \in \mathcal{S}$, a predictors (or regressors) matrix X and a target matrix Y are obtained. Given a dataset with T observations, a prediction horizon of h steps ahead, and an history embedding of e steps, we obtain the Hankel matrix of targets $Y \in \mathbb{R}^{(T-h-e) \times h}$, and the Hankel matrix of the past regressors, $X_p \in \mathbb{R}^{(T-h-e) \times n_x e}$, where n_x is the number of regressors. Verbosely, X_p and Y can be written as:

$$X_p = \begin{bmatrix} x_{1,t-e} & x_{1,t-e+1} & \dots & x_{1,t} & x_{2,t-e} & \dots & x_{n_x,t} \\ x_{1,t-e+1} & x_{1,t-e+2} & \dots & x_{1,t+1} & x_{2,t-e+1} & \dots & x_{n_x,t+1} \\ x_{1,T-2h} & x_{1,T-2h+1} & \dots & x_{1,T-h} & x_{2,T-2h} & \dots & x_{n_x,T-h} \end{bmatrix} \quad (26)$$

$$Y = \begin{bmatrix} y_{t+1} & y_{t+2} & \dots & y_{1,t+h} \\ y_{T-h+1} & y_{T-h+2} & \dots & y_T \end{bmatrix} \quad (27)$$

where $x_{1,t}$ stands for the first regressor at time t . In hour case, we fixed $h = 288$, corresponding to a prediction horizon of 24 hours ahead with a 5 minutes sampling time. The past regressors matrix X_p is then augmented with categorical time features, e.g. day of week, and NWP variables, to obtain the final regressors matrix X .

Holt-Winters model with double seasonality The Holt-Winters (HW) model [7] is a special class of the exponential smoothing [8], which consists of three smoothing equations, such that the final prediction is a combination of the level a , trend b and seasonality s . We tested different flavors of the HW families and based on

performance, we adopted a double seasonality additive HW:

$$\begin{aligned}
\hat{y}_{t+h} &= (a_t + hb_t) + s_{1,t-p(1)+1+(h-1)\backslash p_1} + s_{2,t-p_2+1+(h-1)\backslash p_2} \\
a_t &= \alpha(y_t - s_{1,t-p_1} - s_{2,t-p_2}) + (1 - \alpha)(a_{t-1} + b_{t-1}) \\
b_t &= \beta(a_t - a_{t-1}) + (1 - \beta)b_{t-1} \\
s_{1,t} &= \gamma_1(y_t - a_t - s(2, t - p_2)) + (1 - \gamma_1)s_{1,t-p_1} \\
s_{2,t} &= \gamma_2(y_t - a_t - s(1, t - p_1)) + (1 - \gamma_2)s_{2,t-p_2}
\end{aligned} \tag{28}$$

where α , β , γ_1 and γ_2 are parameters to be learned from data, while $p_1 = 96$ and $p_2 = 672$ are the periods of the seasonalities, and \backslash is the modulo operator. The values for p_1 and p_2 correspond to a daily and weekly period. The model (28), and HW in general, do not include exogenous inputs. Since quantities like external temperature and irradiance are important explanatory variables in load forecasting, we included them with an a-priori linear detrend, such that the new target is $y = y - X\beta_d$, where X is a three column matrix containing GHI , T and the unit vector (for the intercept), and β_d is the vector of linear coefficients. Usually, a single set of α , β , γ_1 and γ_2 values is fitted, and the prediction of each step ahead is obtained applying equations 28 recursively, as usually done for state-space systems. To increase the accuracy of the method, we instead fitted 5 different models: the first two models have the only purpose of predicting the first and second step ahead, respectively. The third model predicts the steps from the third to the fifth, the fourth model predicts the steps up to the 20th and the last one predict the resto of the steps up to 288. Each model has its own set of parameters, which were fitted through random search with a budget of 3000 samples. Since the trend of the time series was negligible, we fixed the β parameters to 0.

Single GBM A single gradient boosted model was fitted to predict all the 288 steps ahead. In order to obtain this, we stacked 288 copies of the features matrix (26), each one decorated with an additional column containing the number of the step ahead to predict. The target was replaced with the opportune reshape of matrix (1.4.3), $\tilde{Y} \in \mathbb{R}^{(T-h-e)h}$.

Independent GBMs In this approach, we fitted 288 models, each one taking as input the same matrix (26), but predicting different columns of (1.4.3). This allows the model to be more expressive (having much more parameters w.r.t. the single model strategy; as we will see this is especially beneficial for the first steps predictions. The drawback is an increase of computational time.

Independent GBMs with Huber loss In figure 5, 1 month power profiles of 4 buildings are aggregated in boxen plots based on the hour of the day, and plotted along with observations (black dots). As can be seen, the distribution at each hour of the day is severely skewed, approaching a bi-modal distribution for night hours. In the literature, prediction of unbalance data is usually threaded with the use of tweedie

loss [9]; however, this approach is useful only in the case of extremely unbalance and zero inflated data, which is not the case as we can see in figure 5. In an attempt to make the model more robust against outliers, we fitted independent GBMs using Huber loss with standard parameters.

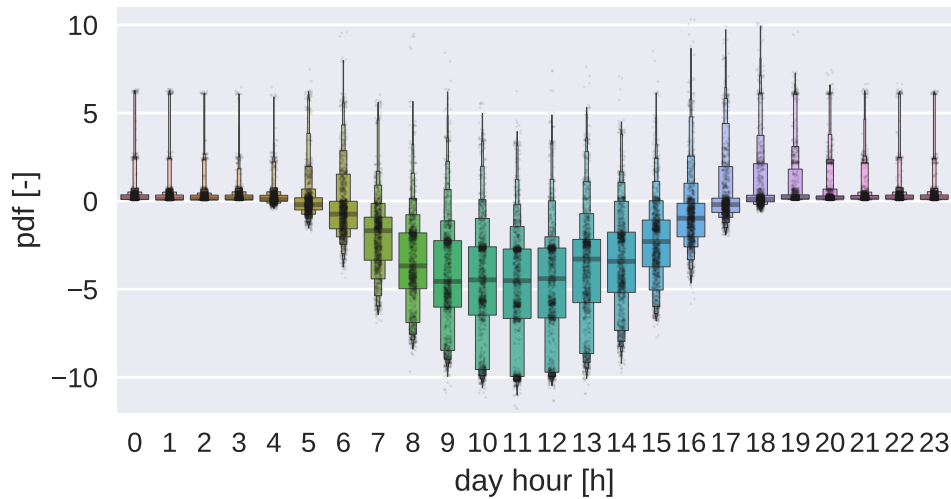


Figure 5: Boxen plots and observations (black dots) of the power distributions of 4 controlled buildings. The observations are groped by hour of the day. The w analyzed buildings has roof-mounted PV plants. All day hours present skewed, but different, distributions.

Hybrid GBMs This final model is an hybrid approach between the Single GBM and the independent GBMs approach. We fitted 5 independent models for the first steps ahead, which we expected to be more important in terms of controllers' performances, and a single GBM for the rest of the steps.

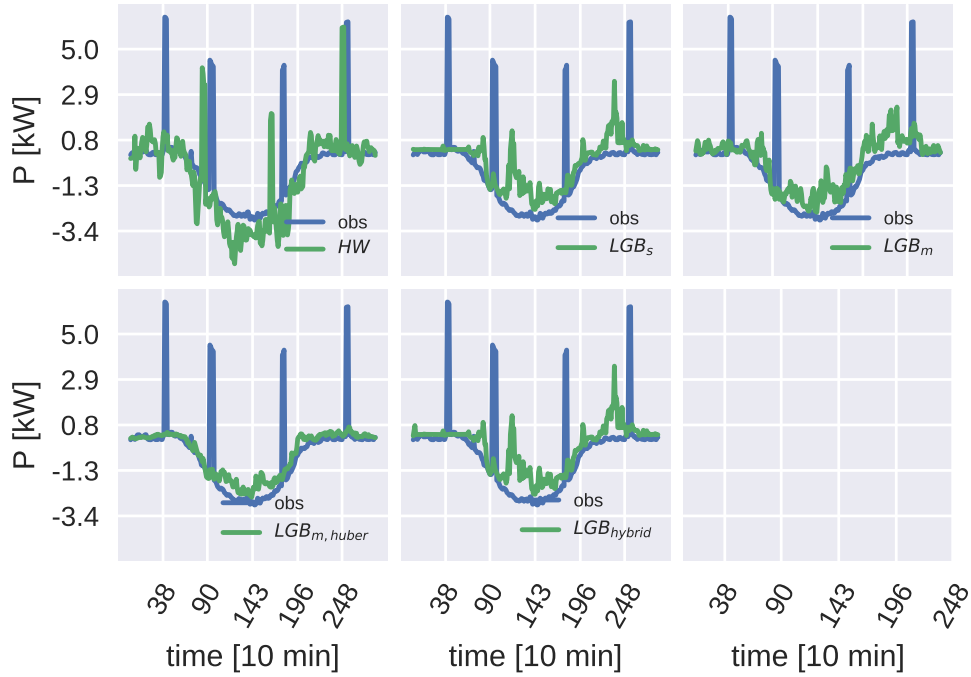


Figure 6: Example of predictions for an household main’s power profile, for the tested forecasters.

1.4.4 Forecasting accuracy

The forecasting accuracy was tested on a 1 month simulation. Figure 6 shows an example of day ahead predictions for the household’s power profile of one of the controlled agents. It can be noticed that the HW model is able to approximately predict the high power peaks due to the presence of an electric boiler, capturing the seasonality of the time series. At the same time, since the turn on events of the boiler are not exactly periodic, the other models tend to underestimate the power profile, actually treating the turn on events as outliers.

More insight can be given by plotting the expected mean absolute error (MAE) of the different forecasters as a function of the day hour (vertical axis) and 5 minutes ahead time of the prediction (horizontal axis), as done in figure 7. For all the methods, we can see that the combination of step ahead and step of the day close to the antidiagonal present the lowest values in terms of MAE. This means that in a time window of a few hours centred around midnight, the predictability of the signal is high. While the non-parametric models are in general better than the HW, the approach using multiple independent models trained with Huber loss do not improve upon the others; this means that treating the turn on of big electric appliances as outliers doesn’t improve the overall MAE. The effect of having several models for the initial steps of the HW based forecaster is clearly visible. This is also visible for the hybrid LGB model, and is better seen in figure 8.

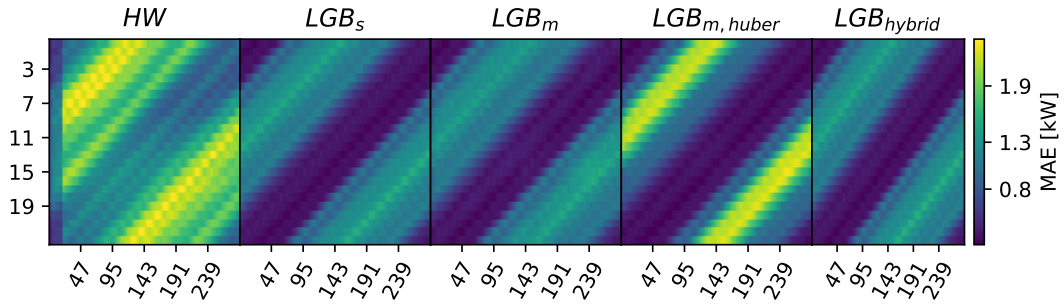


Figure 7: Results in terms of MAE for the households with controlled batteries. The results were mediated using bins of day hour (vertical axis) and 5 minutes ahead time of the prediction (horizontal axis).

Here the MAE for the different forecasters is plotted as a function of step ahead (left) and the time of the prediction (right). The best forecaster in predicting the first step ahead is the HW based forecaster. The independent GBM models and the hybrid approach achieved similar accuracy for the first step, while using the Huber loss deteriorated the performances. In general the hybrid approach combines the first step accuracy of the independent models forecaster with the more stable accuracy of the single GBM forecaster for successive steps ahead. Plotting the MAE as a function of the prediction time highlight the more stable predictions of the non-parametric models w.r.t. the HW model, which is less accurate when predicting the next day ahead during post meridian hours.

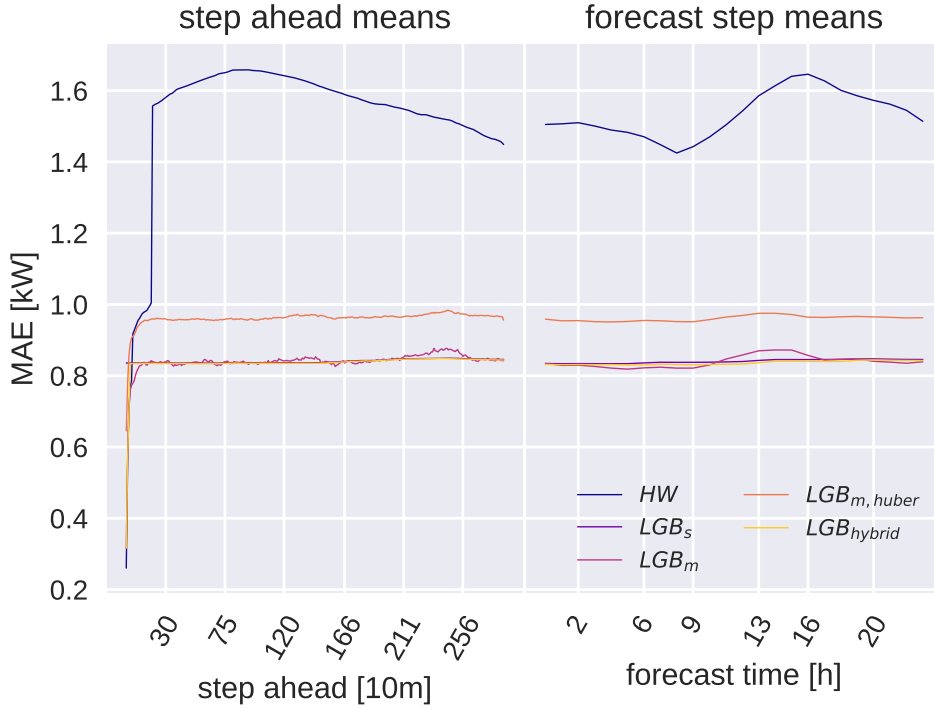


Figure 8: Mean results in terms of MAE for the households with controlled batteries. Left: results mediated on the step ahead. Right: results mediated on the time of the day on which the forecast was performed.

1.4.5 Closed loop performances

Economic results Figure 10 and 9 show the differences in monthly costs with respect to the business as usual, in the case of the explicit and implicit control strategies, for different forecasters. Additionally, we tested the HW and LGB hybrid models in the case in which the battery's constraint for which it cannot charge nor inject in the main grid are removed. In this last case, the battery complementarity constraint on charging and discharging operations is modeled with an integer variable and a big M formulation. For both the business models the change in costs w.r.t. the base case is always positive (meaning a lower cost w.r.t. the base case), as expected since the methods guarantee a reduction of costs for the end-users by construction. The reduction of costs is higher for households with batteries since those are the only controllable devices in this test. The outlier in both plots is the kindergarten, in which a 27 kWp photovoltaic system and a battery with a capacity of 60 kWh are installed. For the implicit coordination, figure 10, no substantial difference is seen among the forecasters, in terms of distribution means. For the explicit coordination case, the cost reduction for the HW is slightly higher in expectation. A more meaningful comparison can be done plotting the differences for the HW and LGB hybrid forecasters, in the case in which injection and charging into e from the grid are allowed for batteries, which is shown in 11 and 12 for the implicit and explicit

coordination cases, respectively. Both for the implicit and the explicit coordination cases, two households with a boiler and a battery worsen their performance when using HW forecaster, w.r.t. the case in which the battery can't inject or charge in and from the grid. Since the relaxed problem allows the battery to perform arbitrage, expanding the feasible space for charging and discharging operations, this can be due to the low accuracy of the HW forecaster for the higher steps-ahead. This hypothesis is strengthened by the fact that the LGB hybrid forecaster, which has a higher accuracy w.r.t. the HW model for higher steps-ahead, shows a consistent decrease of costs for the end-users with a battery. While for the implicit coordination the LGB hybrid model guarantee a reduction in monthly costs for all the participants, this is not the case for the explicit coordination, in which agents without a battery see a slight increase of costs w.r.t. the case in which batteries cannot interface with the main grid. This is due to the redistribution model for the explicit coordination presented in section 1.4.1, which incentives those agents which had a greater impact in reducing the surplus function of the SCC.

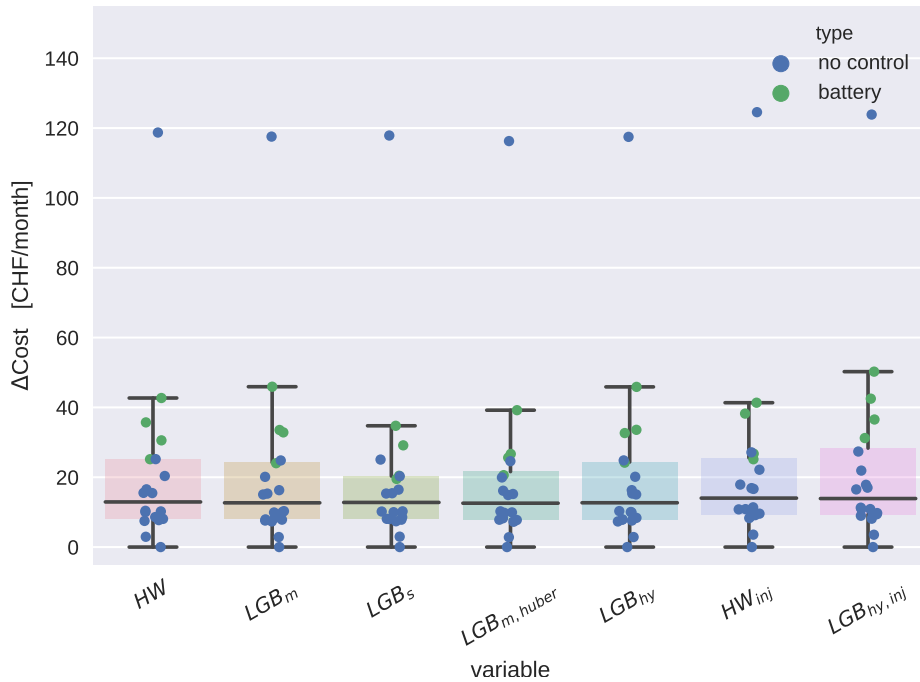


Figure 9: Difference in monthly costs w.r.t. the BaU, for the implicit coordination.

Effect on power at PCC Figure 13 shows the effect of the different forecasting algorithms on the distribution at the PCC. The HW model is surprisingly good at coordinating batteries when the uncontrolled power at the PCC is in its extreme quantiles. The second-best performer in terms of effectiveness in coordination when the PCC power is at extreme values is the hybrid GBM. This suggests that the accuracy of the prediction of the first step ahead is the most important factor when considering grid constraints. Figure 14 shows the pdf of the power at the PCC,

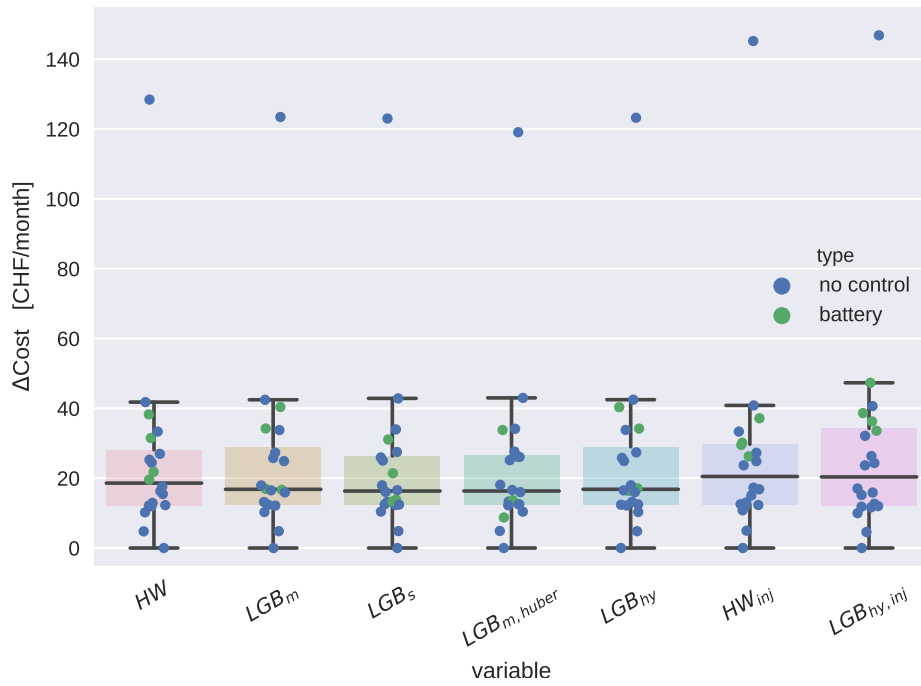


Figure 10: Difference in monthly costs w.r.t. the BaU, for the explicit coordination.

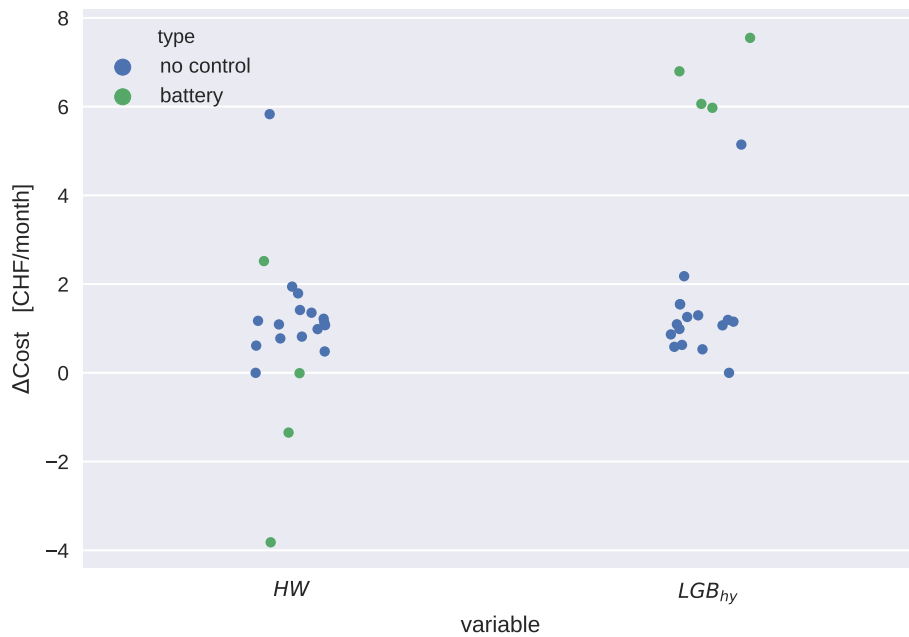


Figure 11: Difference in monthly costs w.r.t. the BaU with no allowed injections, with implicit coordination.

which gives a more complete overview of the different performances of the forecasting models. Once again, it's clear that the best models for reducing the variance of the power at the PCC are the HW and the hybrid GBM models.

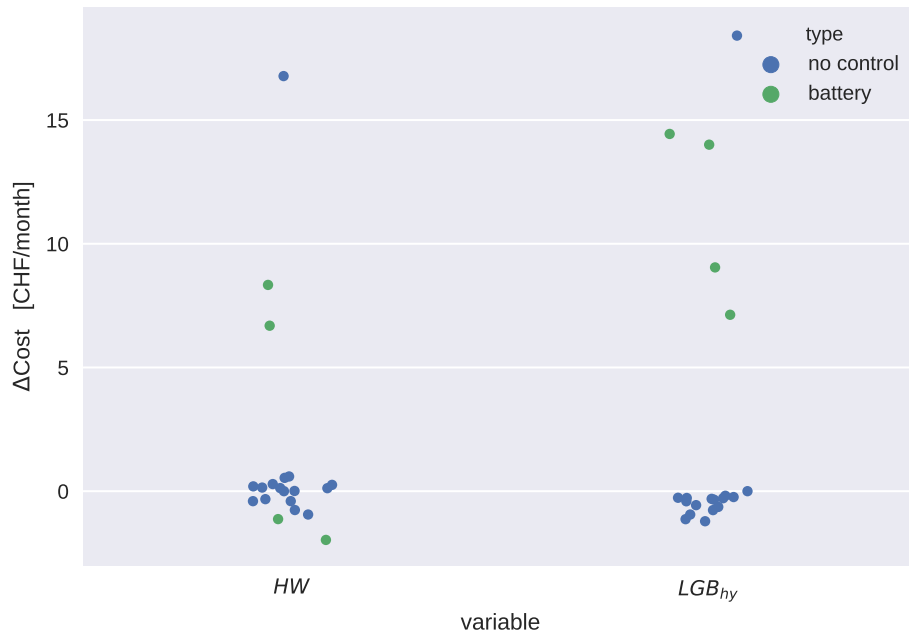


Figure 12: Difference in monthly costs w.r.t. the BaU with no allowed injections, with explicit coordination.

1.5 Regulatory and legal barriers for implementation

The energy schemes proposed in 1.4.1 generate costs which depend on the consumption of all the energy community participants. That is, it is not directly proportional to the energy consumed by the end user, and its get lower when the self consumption inside the energy community increases. Switzerland is embracing a causal principle on the price formation for end users, as stated in the recent modification to the Federal Electricity Supply Act [10]. This means that the electrical bills “should reflect costs caused by end users”. However, the Electricity Supply Ordinance [11] states that DSO must guarantee to the end users that at least 70% of their bills are directly proportional to their energy use; at the same time they can offer opt-in tariffs in which this percentage is reduced. Under these constraints, the tariff proposed in 1.4.1 can be potentially applied in Switzerland.

2 Achievement of deliverable

2.1 Date

November 2020.

2.2 Demonstration of the deliverable

This deliverable presents the impact of different control methods for DSM using communication and different forecasting models. The main features of the developed applications are presented in the previous sections.

3 Impact

The work presented in this deliverable demonstrate the economic feasibility of using distributed control as a tool for reducing the impact of

References

- [1] L. Nespoli and V. Medici, "Constrained hierarchical networked optimization for energy markets," in *Proceedings - 2018 IEEE PES Innovative Smart Grid Technologies Conference Europe, ISGT-Europe 2018*, 2018.
- [2] L. Nespoli, M. Salani, and V. Medici, "A rational decentralized generalized Nash equilibrium seeking for energy markets," in *2018 International Conference on Smart Energy Systems and Technologies, SEST 2018 - Proceedings*, 2018.
- [3] M. Hong, Z. Q. Luo, and M. Razaviyayn, "Convergence analysis of alternating direction method of multipliers for a family of nonconvex problems," *SIAM Journal on Optimization*, vol. 26, pp. 337–364, 2016.
- [4] L. S. Shieh, H. Wang, and R. E. Yates, "Discrete-continuous model conversion," *Topics in Catalysis*, 1980.
- [5] L. Nespoli, "MODEL BASED FORECASTING FOR DEMAND RESPONSE STRATEGIES," Ph.D. dissertation, 2019.
- [6] L. Nespoli, V. Medici, K. Lopatichki, and F. Sossan, "Hierarchical demand forecasting benchmark for the distribution grid," *Electric Power Systems Research*, vol. 189, no. August, p. 106755, 2020. [Online]. Available: <https://doi.org/10.1016/j.epsr.2020.106755>
- [7] C. C. Holt, "Forecasting seasonals and trends by exponentially weighted moving averages," *International Journal of Forecasting*, 2004.
- [8] E. S. Gardner, "Exponential smoothing: The state of the art," *Journal of Forecasting*, 1985.
- [9] H. Zhou, W. Qian, and Y. Yang, "Tweedie gradient boosting for extremely unbalanced zero-inflated data," *Communications in Statistics: Simulation and Computation*, 2020.
- [10] "LAEI 734.7, <https://www.admin.ch/opc/it/classified-compilation/20042411/index.html>."
- [11] "OAEI 734.71, <https://www.admin.ch/opc/it/classified-compilation/20071266/index.html>."

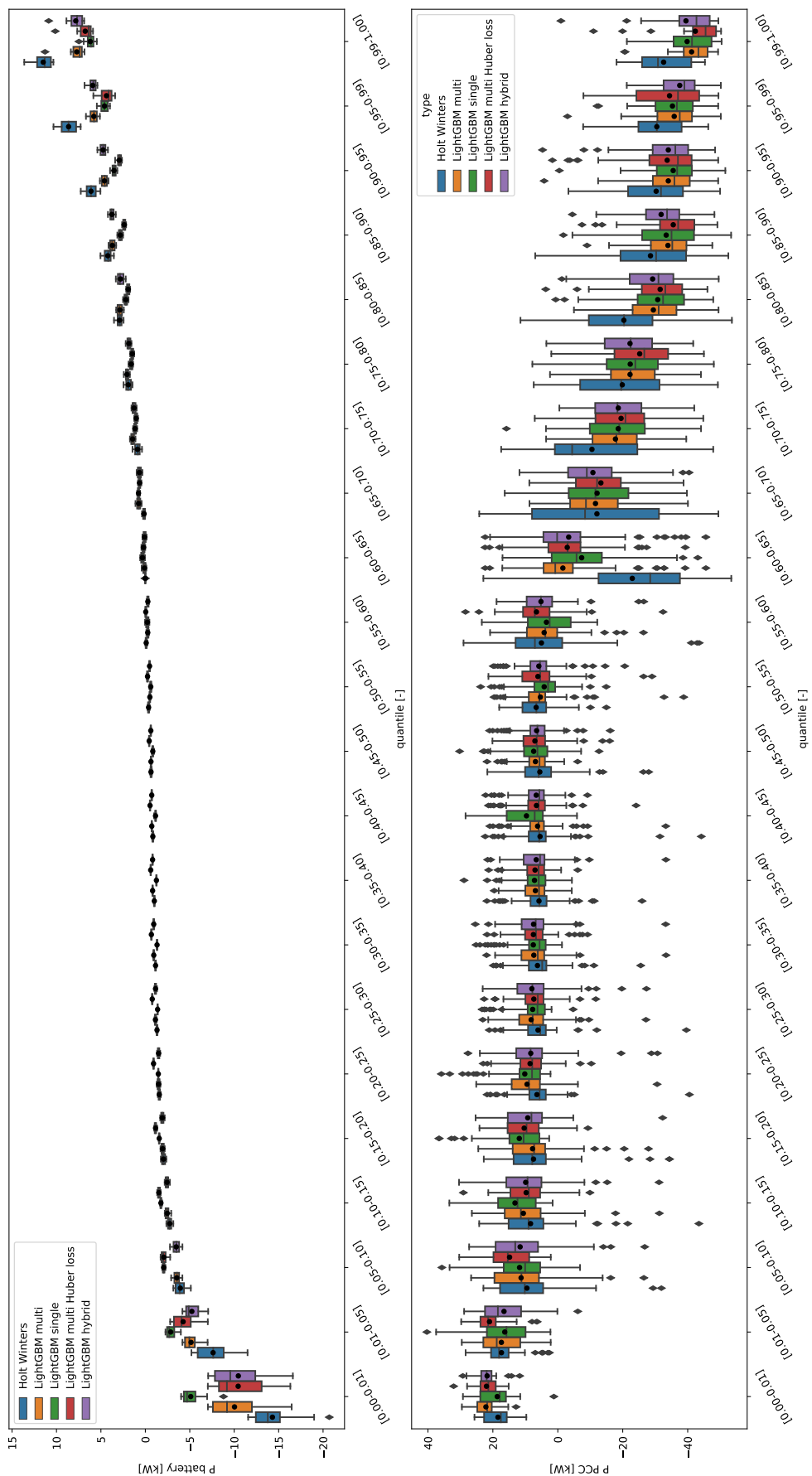


Figure 13: Effect of the different forecasting algorithms coupled with battery control on the power at the point of common coupling (PCC) of the community. Top: boxplots of the power at the PCC per inter-quantile range. Bottom: boxplot of the total power of the batteries per inter-quantile range of the power at the PCC.

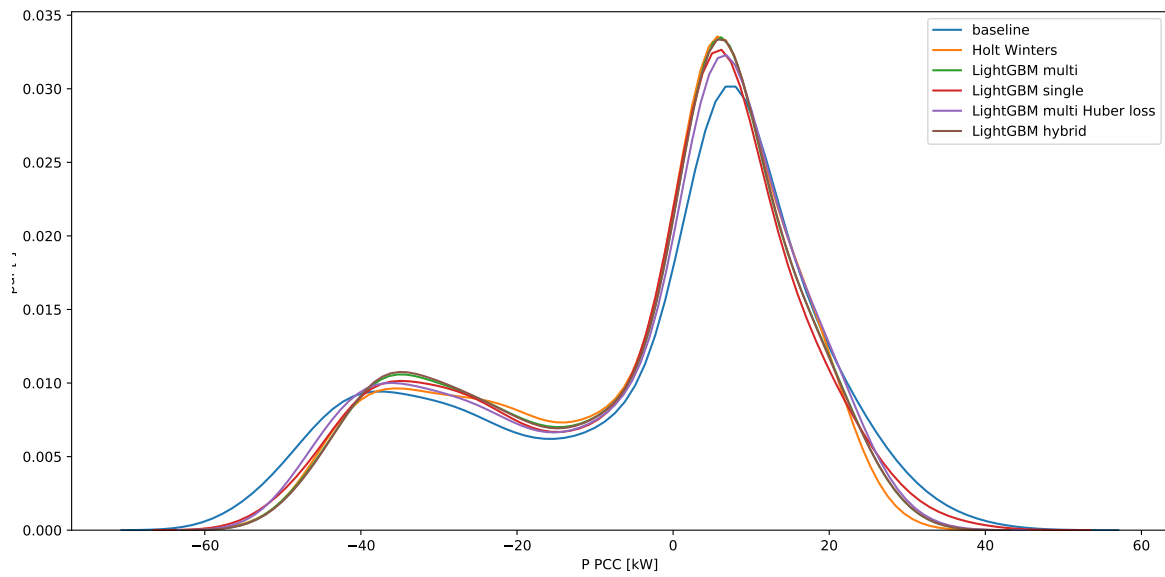


Figure 14: Probability density function (PDF) of the power at the PCC using different forecasting algorithms.